



# JAAS

## Three Dimensional Secondary Ion Mass Spectrometry Imaging (3D-SIMS) of *Aedes aegypti* ovarian follicles

Journal:	<i>Journal of Analytical Atomic Spectrometry</i>
Manuscript ID	JA-ART-12-2018-000425.R2
Article Type:	Paper
Date Submitted by the Author:	20-Feb-2019
Complete List of Authors:	Castellanos, Anthony; Florida International University, Chemistry and Biochemistry Ramirez, Cesar; Florida International University, Michalkova , Veronika ; Florida International University, Chemistry and Biochemistry Nouzova, Marcela; Florida International University, Chemistry and Biochemistry; Institute of Parasitology, Biology Centre CAS Noriega , Fernando; Florida International University, Chemistry and Biochemistry; Florida International University, Biomolecular Sciences Institute Fernandez-Lima, Francisco; Florida International University, Chemistry and Biochemistry; Florida International University, Biomolecular Sciences Institute

SCHOLARONE™  
Manuscripts

1  
2  
3 **1 Three Dimensional Secondary Ion Mass Spectrometry Imaging (3D-SIMS) of**  
4 **2 *Aedes aegypti* ovarian follicles**  
5  
6  
7 3  
8  
9

10 4 Anthony Castellanos<sup>1</sup>, Cesar E. Ramirez<sup>1</sup>, Veronika Michalkova<sup>2</sup>, Marcela Nouzova<sup>2,3</sup>, Fernando  
11  
12 5 G. Noriega<sup>2,4</sup> and Francisco Fernández-Lima<sup>1,4\*</sup>  
13  
14

15 6 <sup>1</sup>Department of Chemistry and Biochemistry, Florida International University, Miami, Florida,  
16  
17 7 33199, United States; <sup>2</sup>Department of Biological Sciences, Florida International University,  
18  
19 8 Miami, Florida, 33199, United States; <sup>3</sup> Institute of Parasitology, Biology Centre CAS, Ceske,  
20  
21 9 Budejovice, Czech Republic; and <sup>4</sup>Biomolecular Sciences Institute, Florida International  
22  
23 10 University, Miami, Florida, 33199, United States.  
24  
25  
26  
27  
28 11  
29  
30

31 12 \*Corresponding author: Francisco A. Fernández-Lima, Department of Chemistry and  
32  
33 13 Biochemistry, Florida International University, 11200 SW 8th St AHC4-233, Miami, FL 33199,  
34  
35 14 USA; *e-mail*: [fernandf@fiu.edu](mailto:fernandf@fiu.edu)  
36  
37  
38  
39 15  
40  
41  
42 16  
43  
44

45 17 Keywords: SIMS, lipids, mass spectrometry, mosquitoes, ovary, imaging  
46  
47  
48  
49  
50  
51  
52  
53  
54  
55  
56  
57  
58  
59  
60

1  
2  
3 **18 Abstract**  
4  
5

6 19 The mobilization of nutrient reserves into the ovaries of *Aedes aegypti* mosquitoes after sugar-  
7  
8 20 feeding plays a vital role in female's reproductive maturation. In the present work, three-  
9  
10 21 dimensional secondary ion mass spectrometry imaging (3D-SIMS) was used to generate ultrahigh  
11  
12 22 spatial resolution (~1  $\mu\text{m}$ ) chemical maps and study the composition and spatial distribution of  
13  
14 23 lipids at the single ovarian follicle level (~100  $\mu\text{m}$  in size). 3D-Mass Spectrometry Imaging (3D-  
15  
16 24 MSI) allowed the identification of cellular types in the follicle (oocyte, nurse and follicular cells)  
17  
18 25 using endogenous markers, and revealed that most of the triacylglycerides (TGs) were  
19  
20 26 compartmentalized in the oocyte region. By comparing follicles from water-fed and sugar-fed  
21  
22 27 females (n=2), 3D-MSI-Time of Flight-SIMS showed that TGs were more abundant in ovarian  
23  
24 28 follicles of sugar-fed females; despite relative sample reproducibility per feeding condition, more  
25  
26 29 biological replicates will better support the trends observed. While the current 3D-MSI-TOF-SIMS  
27  
28 30 does not permit MS/MS analysis of the lipid species, complementary LC-MS/MS analysis of the  
29  
30 31 ovarian follicles aided tentative lipid assignments of the SIMS data. The combination of these MS  
31  
32 32 approaches is giving us a first glimpse on the distribution of functionally relevant ovarian lipid  
33  
34 33 molecules at the cellular level. These new tools can be used to investigate the roles of different  
35  
36 34 lipids on follicle fitness and overall mosquito reproductive output.  
37  
38  
39  
40  
41  
42  
43  
44  
45  
46  
47  
48  
49  
50  
51  
52  
53  
54  
55  
56  
57  
58  
59  
60

## 36 Introduction

37 Mass spectrometry-based techniques are the analytical gold standard for the separation,  
38 identification, and quantification of lipids in biological samples. [1, 2] Typically, total lipid  
39 analysis by MS is based on extraction protocols from biological matrices followed by liquid  
40 chromatography coupled to tandem mass spectrometry (e.g., LC-MS/MS). [3, 4] However,  
41 depending on the biological question, the chemical mapping the lipid distribution in biological  
42 systems using mass spectrometry imaging (MSI) techniques is mandatory. For example, liquid  
43 based junctions, jets and micro-junctions (i.e., liquid extraction surface analysis, or LESA), [5, 6]  
44 desorption electrospray ionization (DESI), [7, 8] and nanospray desorption electrospray ionization  
45 (nano-DESI) [9] can provide lipid chemical maps with spatial resolution down to ~600  $\mu\text{m}$ , ~50  
46  $\mu\text{m}$ , [10, 11] and ~10  $\mu\text{m}$ , [12] respectively, under ambient conditions and without the need of any  
47 surface treatment. Other MSI techniques using laser sources can provide a higher spatial resolution  
48 (10-50  $\mu\text{m}$  or down to few  $\mu\text{m}$  using special arrangements [13]) at ambient or vacuum conditions,  
49 but typically require the coating of the biological surfaces with a matrix (i.e., MALDI [14-16]);  
50 the matrix choice and application method determine the selectivity of analytes and the crystal size  
51 can become the limiting factor of the spatial resolution [16, 17]. For MSI lipid analysis with high  
52 spatial resolution (<1  $\mu\text{m}$ ) [18-21], ion beams are typically used under vacuum conditions [22]  
53 without the need of surface treatment (i.e., secondary ion mass spectrometry, SIMS) [23]; SIMS  
54 spatial resolution and secondary ion yield varies with the projectile size (e.g., from atomic to poly-  
55 atomic to cluster beams) and incident energy. [24-33]

56 Lipid MSI has been mainly performed by 2D imaging of subsequent sample sections, with  
57 consequent loss of 3D information due to the thickness of each slide (typically tens of  $\mu\text{m}$ ).  
58 Alternatively, with the advent of “soft” ion probes (e.g., fullerenes, [34-36] argon clusters, [37,

1  
2  
3 59 38] water clusters, [39] and carbon dioxide clusters [40]), MSI can interrogate biological surfaces  
4  
5 60 “layer by layer” (nanometer depth resolution) with ultrahigh spatial resolution using SIMS [41].  
6  
7  
8 61 In particular, 2D and 3D SIMS are exceptionally suited for the lipid study of small and complex  
9  
10 62 biological samples such as insects at the single cell level. [42-45]  
11  
12

13 63 Lipids are extremely important for the development and reproduction of *Ae. aegypti* mosquitoes.  
14  
15 64 The nutritional and hormonal regulation of reproduction is a critical component of mosquito  
16  
17 65 female fitness, and therefore of the ability to transmit diseases. [46-48] Mosquito-borne diseases  
18  
19 66 such as Zika, Dengue, Chikungunya and Malaria constitute critical threats to public health in many  
20  
21 67 parts of the world. [49-52] Each of the two ovaries of the female of *Ae. aegypti* mosquitoes contains  
22  
23 68 about 60 ovarioles with germaria attached to primary and secondary follicles. Each follicle consists  
24  
25 69 of one oocyte plus 7 nurse cells that are surrounded by follicular epithelial cells. [53] There are  
26  
27 70 three periods in the development of the primary ovarian follicles during a gonotrophic cycle:  
28  
29 71 previtellogenesis (PVG), ovarian resting stage (ORS) and vitellogenesis (VG). Females emerge  
30  
31 72 with immature primary follicles that grow into mature PVG follicles in the next 48-72 h; oocytes  
32  
33 73 remain in a dynamic “state of arrest”, and will enter VG only after a blood meal. [54] *Ae. aegypti*  
34  
35 74 females can lay over 120 eggs in a gonotrophic cycle; therefore, a tightly regulated control of  
36  
37 75 nutrient allocations to the ovaries is critical for survival. [55, 56] The ovarian resting stage in *Ae.*  
38  
39 76 *aegypti* is a period marked by constant adjustment of the reproductive output based on nutritional  
40  
41 77 status; this adjustment occurs mostly through follicular resorption by apoptosis. [55]  
42  
43 78 During their PVG maturation, mosquito oocytes increase their lipid content several-fold. [57] The  
44  
45 79 main source of lipids for oocytes comes from larval accrual (teneral) reserves, as well as from  
46  
47 80 sugar meals taken by the adult. [58] Female mosquitoes are subject to ‘trade-offs’ between the  
48  
49 81 energetic demands of reproduction and the energy required to survive; they must consider the  
50  
51  
52  
53  
54  
55  
56  
57  
58  
59  
60

1  
2  
3 82 effects of immediate resource allocations on future reproduction and overall fitness. [55, 56] While  
4  
5 83 previous studies have described that high sugar diets prompt accumulation of lipids in the oocyte,  
6  
7  
8 84 [56] little is known about the lipid identities, composition and distribution within a single follicle.  
9  
10 85 In the current study, for the first time, 3D-SIMS is utilized for the analysis of lipid composition  
11  
12 86 and lipid spatial distribution of single follicles from ovaries of *Ae. aegypti* mosquitoes. An  
13  
14 87 organism model that recreates different ovarian phenotypes during the ORS based on a sugar diet  
15  
16  
17 88 is utilized to evaluate the reproductive output and lipid content at the follicle level. Results  
18  
19 89 demonstrated the capability of 3D-SIMS to generate chemical maps with high spatial resolution  
20  
21 90 and the visualization of intact lipids. In particular, we demonstrated that sugar-feeding results in  
22  
23 91 increased levels of polyunsaturated triacylglycerides (TG) with long chain fatty acids, such as TG  
24  
25 92 48:1, 48:2, 50:1 and 50:2; with most of the TGs compartmentalized in the oocyte region.  
26  
27  
28

## 29 93 **Materials and Methods**

### 30 94 *Mosquito samples*

31  
32 95 *Ae. aegypti* of the Rockefeller strain were raised at 28 °C with 80% humidity, at a 16-hour light  
33  
34 96 and 8-hour dark cycle.[55] After adult eclosion, females were fed from either a cotton pad soaked  
35  
36 97 in a 20% sucrose solution or a water-soaked cotton pad (0% sucrose). On the fifth day, females  
37  
38 98 were collected and cold anaesthetized over ice. Ovaries were dissected in phosphate-buffered  
39  
40 99 saline (PBS), stained with a DAPI solution (prepared 3 μM in PBS), and rinsed in a solution of  
41  
42 100 150 mM ammonium acetate adjusted to a pH of 7.4.  
43  
44  
45  
46  
47

### 48 101 *LC-MS/MS Analysis*

49  
50 102 Ten mosquito ovaries were dissected and transferred into a 1.5 mL Eppendorf tube containing 100  
51  
52 103 μL of 50:50 1-butanol/methanol. A 2.5 μL aliquot of a 1 mM solution of the antioxidant butylated  
53  
54 104 hydroxytoluene (BHT) was added to prevent lipid degradation. A mix of several deuterated lipids  
55  
56  
57  
58  
59  
60

1  
2  
3 105 (10  $\mu$ L of Splash Lipidomix, Avanti Polar Lipids, Alabaster, AL) was introduced for internal  
4  
5 106 standarization. Kontes polypropylene pellet pestles (Fisher Scientific, Pittsburgh, PA) were used  
6  
7 107 with a cordless motor to mechanically homogenize ovaries for 10 seconds. The pestle was then  
8  
9 108 rinsed with 200  $\mu$ L of 1-butanol/methanol. Samples were sonicated for 30 minutes at room  
10  
11 109 temperature, and centrifuged at 1600 $\times$ g for 10 minutes. The supernatants were then transferred  
12  
13 110 into 2 mL autosampler silanized vials (Thermo Fisher Scientific, Waltham, MA).

14  
15 111 LC-MS/MS analyses were performed on a Prominence LC-20 CE Ultra-Fast Liquid  
16  
17 112 Chromatograph (Shimadzu, Kyoto, Japan) equipped with a Dionex Acclaim C18 Column (250  $\times$   
18  
19 113 2.1 mm, 5  $\mu$ m) (Thermo Scientific, Sunnyvale, CA), performing gradient separations between  
20  
21 114 40:60 ACN:water and 89:10:1 solution of isopropyl alcohol (IPA):ACN:water (both with 10 mM  
22  
23 115 ( $\text{NH}_4\text{COOH}$ ) and 0.1% FA).

24  
25 116 Detection was performed by a Bruker timsTOF quadrupole-time of flight (QTOF) mass  
26  
27 117 spectrometer (Billerica, MA) equipped with an electrospray ionization source. The instrument was  
28  
29 118 operated under data-dependent scan acquisition mode, performing MS/MS via collision induced  
30  
31 119 dissociation (CID). Lipid candidate assignments were made using Metaboscape (Bruker Daltonics  
32  
33 120 Inc.) and SimLipid (PREMIER Biosoft, Palo Alto, CA). MS/MS assignments were manually  
34  
35 121 curated and a 10 ppm tolerance was used for MS<sup>1</sup>.

#### 36 122 *Follicle Freeze-Drying Procedure*

37  
38 123 Follicles were prepared using a freeze-drying method, [18] optimized here for fluorescence  
39  
40 124 imaging and 3D-TOF-SIMS analysis. Ovaries were first placed in a 150 mM ammonium acetate  
41  
42 125 droplet on an ITO coated glass slide, and individual follicles were mechanically separated using  
43  
44 126 microdissection pins. The droplet containing ovarian follicles was sandwiched with a second ITO  
45  
46 127 slide, using glass coverslips as a spacer ( $\sim$ 20  $\mu$ m) on either end. The assembly was held in place  
47  
48  
49  
50  
51  
52  
53  
54  
55  
56  
57  
58  
59  
60

1  
2  
3 128 using binder clips, and subsequently immersed in liquid nitrogen for several minutes. The binder  
4  
5 129 clips were then removed, and the ITO slides were separated while still immersed in liquid nitrogen,  
6  
7  
8 130 akin to freeze-fracture techniques. [59] The sample slides were then transferred into a custom-built  
9  
10 131 vacuum dryer and allowed to dry as liquid nitrogen boiled off and returned to room temperature.  
11  
12 132 The sandwich technique employed here allowed for follicles to remain relatively flat and attached  
13  
14 133 to the slide, enabling subsequent microscopy. Afterwards, ITO slides were mounted on an ION-  
15  
16 134 TOF top mount stage for TOF-SIMS analysis. The use of ammonium salts for washing and freeze-  
17  
18 135 drying have been previously utilized to prevent the accumulation of non-volatile salts such as  
19  
20 136 sodium and potassium, commonly present in buffer solutions. [60] In addition, freeze-drying  
21  
22 137 preserves cell morphology without the use of chemical fixatives or alcohol dehydration, which  
23  
24 138 could cause a displacement of diffusible ions and membrane phospholipids. [61, 62]  
25  
26  
27

### 28 139 *Microscopy*

29  
30  
31 140 Following the freeze-drying of ovarian follicles, sample slides were inspected with a Nikon  
32  
33 141 Eclipse Ts2R-FL inverted microscope (Nikon Instruments Inc., Melville, NY). Phase contrast  
34  
35 142 images were recorded with a  $\times 20$  objective using a 30 ms exposure time. A Nikon DAPI filter  
36  
37 143 was used to visualize stained ovarian follicles at an exposure time of 600 ms. Observations of  
38  
39 144 freeze-dried samples revealed that our sample preparations yielded relatively flat individual  
40  
41 145 follicles, with most fluorescent nurse cells in focus and minimal instances of fractures.  
42  
43  
44

### 45 146 *3D-TOF-SIMS Analysis*

46  
47 147 A TOF-SIMS 5 instrument retrofitted with a 25 kV Bismuth liquid metal ion gun and a 20 kV  
48  
49 148 argon cluster sputtering (ION-TOF GmbH, Münster, Germany) was used. The 3D-TOF-SIMS  
50  
51 149 spectra were collected in High Current Bunched mode (HCBU). 2D-MSI analyses were performed  
52  
53 150 by rastering a  $\text{Bi}_3^+$  primary ion beam over a  $200 \times 200 \mu\text{m}^2$  area centered on the ovarian follicles.  
54  
55  
56  
57  
58  
59  
60



1  
2  
3 151 Total 2D-MSI primary ion doses were  $\sim 1 \times 10^{12}$  ions $\cdot$ cm $^{-2}$  per sputter cycle, with a measured spatial  
4  
5 152 resolution of  $< 3$   $\mu$ m. The 20 keV argon cluster ion beam (Ar $_{2200}^+$ ) was used to sputter the sample  
6  
7 153 surface at an ion dose of  $\sim 1 \times 10^{13}$  ions $\cdot$ cm $^{-2}$  in between 2D-MSI scans. That is, the 3D-MSI data  
8  
9 154 consisted of non-interlaced cycles of Bi $_3^+$  and Ar $_{2200}^+$  ion bombardment. After the samples  
10  
11 155 substrate was reached during the 3D analysis, the summed signals from all 3D voxels were used  
12  
13 156 for 2D visualization and quantification. 3D-TOF-SIMS analyses were carried out in duplicate on  
14  
15 157 follicles from either diet. Ion beam-induced charge accumulation on the sample surface was  
16  
17 158 compensated with an electron flooding gun (21 eV). Secondary ions were accelerated to a kinetic  
18  
19 159 energy of 3 KeV toward a field-free region and a single-stage reflectron. Secondary ions were  
20  
21 160 post-accelerated to a kinetic energy of 10 KeV, before reaching a hybrid detector, composed of a  
22  
23 161 multichannel plate scintillator, and a photomultiplier detection system. In the positive polarity,  
24  
25 162 mass spectra were internally calibrated using the commonly observed hydrocarbon series: C $^+$ , CH $^+$ ,  
26  
27 163 CH $_2^+$ , CH $_3^+$ , C $_2$ H $_3^+$ , and C $_2$ H $_5^+$ , as well as the commonly observed lipid fragment ions C $_5$ H $_{14}$ NO $^+$   
28  
29 164 and C $_5$ H $_{15}$ NPO $_4^+$ . [30] A mass resolution of R=3000 at 851  $m/z$  (TG 50:3 [M+Na] $^+$  ion) was  
30  
31 165 observed during the positive mode HCBU analysis. TOF-SIMS signals were labeled based on LC-  
32  
33 166 MS/MS analysis from replicate samples with a mass tolerance of 10 ppm in MS $^1$  and with MS/MS  
34  
35 167 information. A TOF-SIMS mass accuracy of  $< 100$  ppm, attributed to the non-flat nature of the  
36  
37 168 sample, was observed for all annotated PC and TG.  
38  
39 169 Data were collected and processed using the ION-TOF SurfaceLab 6 V6.4 (Münster, Germany).  
40  
41 170 The NESAC/BIO's NBToolbox V2.7 software (available at <http://mvsa.nb.uw.edu>) was used to  
42  
43 171 correct the z-axis and reconstruct depth profile data assuming a constant sputter rate.  
44  
45 172 Secondary ion yields ( $Y_{SI}$ ) were calculated by normalizing the secondary ion intensity to the  
46  
47 173 fluence of the primary ion beam and to the size of the region of interest (ROI) for direct  
48  
49  
50  
51  
52  
53  
54  
55  
56  
57  
58  
59  
60

1  
2  
3 174 comparison between 3D-MSI scans of the sample composition. [18] That is, fluctuations in the  
4  
5 175 primary ion beam and the total 3D interrogated surface area are accounted for and the resulting  
6  
7  
8 176 units for  $Y_{SI}$  are the number of secondary ions detected per primary ion impact.

9  
10  
11 177 
$$Y_{SI\text{follicle}} = \frac{\Sigma \text{Secondary ions}}{\Sigma \text{ROI follicle}(cm^2) \times \text{fluence}\left(\frac{\text{primary ions}}{cm^2}\right)} \quad (1)$$
  
12  
13

## 14 178 **Results and Discussion**

15  
16  
17 179 A fundamental aspect of animal life history is the ability of an organism to convert available  
18  
19 180 resources into usable nutrients and energy for maintenance, activity and reproduction. Lipids are  
20  
21 181 the major form of energy storage in animals, and in insects, lipids imported from circulation  
22  
23 182 provide most of the energy and nutrients required during egg development. [63] In the mosquito  
24  
25 183 *Culex quinquefasciatus*, ~90 % of the energy used during embryogenesis originates from  
26  
27 184 lipids.[64] In *Ae. aegypti*, ~80% of lipids found in eggs are derived from regular sugar meals  
28  
29 185 before blood feeding. [46, 65] To better understand the roles of sugar-feeding derived lipid reserves  
30  
31 186 on mosquito ovarian development, we compared ovarian follicles from water-fed and sugar-fed  
32  
33 187 *Ae. aegypti* females, a mosquito experimental model previously developed to study the effect of  
34  
35 188 nutrition on mosquito reproduction. [55, 56] Females were isolated at adult eclosion, and raised  
36  
37 189 for 5 days on either a 20% sucrose solution or water. Ovaries from sugar-fed females were larger  
38  
39 190 than those from water-fed females, with the oocytes clearly visible with light microscopy (Figure  
40  
41 191 1).

42  
43  
44  
45  
46  
47 192 Our first challenge was to optimize a sample preparation protocol that preserves the structural  
48  
49 193 features of the follicle without interfering with the SIMS analysis. To this end, DAPI staining  
50  
51 194 served as a quality control following the freeze-drying procedure discussed in the methods section.  
52  
53 195 Figure 2 provides a phase contrast and fluorescence image of an ovarian follicle after freeze-  
54  
55 196 drying. As the follicle scheme illustrates, a suitable protocol should allow the visualization of

1  
2  
3 197 several nurse cells surrounded by the follicular epithelium; with the oocyte in a distal position in  
4  
5 198 reference to the secondary follicle and the germarium (Figure 2).  
6

7  
8 199 *Assignment of lipid species*  
9

10 200 After verifying the structural integrity of all samples, follicles from both feeding conditions were  
11  
12 201 subjected to 3D-TOF-SIMS analysis. While the TOF-SIMS platform offers reasonable mass  
13  
14 202 resolution (e.g., <10,000), the complexity of biological samples makes it insufficient for  
15  
16 203 unambiguous chemical formula assignment. [66] Our current 3D-MSI platform does not allow for  
17  
18 204 MS/MS analysis; therefore, replicate samples were analyzed by LC-MS/MS to confirm the  
19  
20 205 identification of lipid species. A comprehensive list of the 3D-TOF-SIMS assignments and the  
21  
22 206 supporting MS<sup>2</sup> information can be found in Table 1. Pseudomolecular secondary ions for  
23  
24 207 phosphatidylcholines (PC) of the form [M+H]<sup>+</sup> and triglycerides (TG) of the form [M+Na]<sup>+</sup> were  
25  
26 208 primarily observed during 3D-TOF SIMS positive ion mode. Lipid species are abbreviated herein  
27  
28 209 according to lipid class and the number of carbons and double bonds along fatty acyl tails is  
29  
30 210 provided. For example, TG (16:1/16:1/16:1) refers to a triacylglyceride with three fatty acyl  
31  
32 211 groups, each with a 16 carbon chain containing only one double bond.  
33  
34  
35  
36  
37

38 212 *3D mapping of lipid species*  
39

40 213 In Figure 3, the summed 3D signals of several PCs and TGs are depicted in green and red,  
41  
42 214 respectively for follicles from sucrose-diet females. The 3D-TOF-SIMS has a major advantage  
43  
44 215 compared to other 3D-MSI techniques, enabling full access to the 3D information. [18, 67] This  
45  
46 216 capability is illustrated in Figure 3, where successive 2D-MSI heat maps are generated with the  
47  
48 217 Bi<sub>3</sub><sup>+</sup> analytical beam between Ar<sub>2200</sub><sup>+</sup> sputtering cycles are visualized. A comprehensive molecular  
49  
50 218 description of species within the follicle is only possible using the 3D-MSI analysis due to the  
51  
52 219 heterogeneity and morphology of the mosquito follicles. Significant advantage when compared to  
53  
54  
55  
56  
57  
58  
59  
60

1  
2  
3 220 other 3D tools (e.g., confocal microscopy) is that 3D-MSI TOF MS allows for the simultaneous  
4  
5 221 detection of multiple  $m/z$  signal. After the samples substrate was reached during the 3D analysis,  
6  
7  
8 222 the summed signals from all 3D voxels were used for 2D visualization and quantification.  
9  
10 223 However, caution should be taken when constructing such 3D-MSIs since sputtering rates depend  
11  
12 224 on the sample composition. For the analysis presented, a z-axis correction relative to the flat  
13  
14 225 substrate was used for a reconstructed visualization of the mosquito follicles (see more details of  
15  
16  
17 226 3D reconstruction of non-flat samples in ref [68]). Supplemental Figure S1 depicts aerial three-  
18  
19 227 dimensional visualization of selected  $m/z$  ions.

20  
21 228 The  $m/z$  of 81.03 was tentatively assigned as  $C_5H_5O^+$ , a fragment ion of ribose previously reported  
22  
23 229 in SIMS analyses of DNA and ribose standards as well as in mammalian cells. [69-71] This  $m/z$   
24  
25 230 of 81.03 ion (blue) was co-located with DAPI-stained nurse cells. Nurse cells synthesize large  
26  
27 231 amounts of RNA, which is transferred to the developing oocyte.

28  
29  
30 232 Sum signal of the 3D-MSI analysis were used to build a complementary 2D representation (top  
31  
32 233 view) of the follicle PCs (green), TGs (red) and ribose ( $m/z$  81.03, blue) signals in Figure 4. When  
33  
34 234 compared to the diagram of the follicle in Figure 1, these species were demonstrated to localize to  
35  
36 235 the follicular epithelium, oocyte, and nurse cells, respectively. Readers are referred to Table 1 for  
37  
38 236 a comprehensive list of the  $m/z$  and their corresponding assignments for PC and TG. Note that  
39  
40 237 different from other imaging techniques where labeling is required, the  $m/z$  channels used to  
41  
42 238 reconstruct the follicle structure are endogenous to the sample. This feature makes 3D-TOF-SIMS  
43  
44 239 a powerful label-free technique for the analysis of biologically relevant molecules.

#### 45 46 47 240 *Polyunsaturated TG contents in ovarian follicles*

48  
49  
50 241 All TGs identified contained either mono- or poly-unsaturated long-chain fatty acids (LCFA) with  
51  
52 242 16-20 carbons in each fatty acyl group (see Table 1). In Figure 5, the secondary ion yield for  
53  
54  
55  
56  
57  
58  
59  
60

1  
2  
3 243 thirteen selected TGs are compared for the two diet conditions. Ovarian follicles from sucrose-fed  
4  
5 244 females exhibited increases in all the detected TGs, with differences between the two diets  
6  
7  
8 245 decreasing as the fatty acid chain length increased (greater differences in TG 48 and 50 vs. TG 52  
9  
10 246 and 54). These studies also revealed that the amounts of poly-unsaturated TGs, such as 50:4, 52:4  
11  
12 247 and 54:4, were less affected by the female diet. SIMS was also used to compare PCs in individual  
13  
14 248 follicles from water- and sugar-fed females. There were not major differences in the signal of PCs  
15  
16  
17 249 from females raised with the two diets in the follicles sampled (Supplemental Figure S2). 3D-MSI  
18  
19 250 trends in TG and PC relative abundances as a function of the diet agree with those from LC-  
20  
21 251 MS/MS measurements. That is, TGs were found to be more abundant in extracts of sucrose-fed  
22  
23  
24 252 female ovaries while no major differences in the PCs between the two diets were observed  
25  
26 253 (Supplemental Figure S2).

27  
28 254 Triacylglycerides are the main lipid class stored in mosquito eggs as a long-term source of energy  
29  
30  
31 255 and nutrients. [72] Sugar-feeding resulted in a higher mobilization of saturated TG into the  
32  
33 256 developing eggs. Previously, mosquito embryonic development has been demonstrated to be  
34  
35 257 completed within ~3 days after oviposition, and fully developed 1st instar larvae reside for  
36  
37  
38 258 weeks/months within the chorion awaiting the appropriate environmental cues to stimulate  
39  
40 259 hatching. [72] Reserves of TG with saturated fatty acids are very stable, whereas unsaturated acids  
41  
42 260 are more susceptible to oxidation; the more double bonds, the greater the susceptibility. Mosquito  
43  
44  
45 261 pharate larvae can withstand months of quiescence inside the egg only depending on these stored  
46  
47 262 “stable” maternal reserves.

48  
49 263 Ovaries from mosquitoes reared under different nutritional conditions showed differences in  
50  
51 264 follicle size, oocyte size, oocyte lipid contents, and overall morphology. Nutritional stress  
52  
53  
54 265 generated a more heterogeneous population of follicles with different intrinsic “quality”,  
55  
56  
57  
58  
59  
60

1  
2  
3 266 including dissimilar lipid reserves. These differences determine the potential of individual follicles  
4  
5 267 for further development, and categorize them into “viable” and “unviable” follicles. [56] Unviable  
6  
7 268 follicles have higher probability of being resorbed by apoptosis, this resorption of follicles  
8  
9  
10 269 represents a reversal of nutrients away from reproduction and towards alternative activities and  
11  
12 270 reflects the need to balance present and future reproduction to maximize fitness. [55, 56, 73]  
13

14  
15 271 **Conclusions:**

16  
17 272 3D-TOF-SIMS analysis allowed for the recognition of different cell types within the mosquito  
18  
19 273 ovarian follicle, as well as revealed changes of lipid species at the individual ovarian follicle level.  
20  
21 274 A good agreement was observed between optical and 3D-TOF-SIMS derived structural features,  
22  
23 275 differentiating the three main follicular components (oocyte, nurse cells, and follicular epithelial  
24  
25  
26 276 cells). Our studies revealed that stored poly-unsaturated TGs increased in sucrose-fed insects; and  
27  
28 277 therefore, these TG species could be used as markers for follicular fitness and overall mosquito  
29  
30  
31 278 reproductive output. Despite relative sample reproducibility per feeding condition, the current  
32  
33 279 analysis consisted of  $n = 2$  and more biological replicates will better support the trends observed.  
34  
35 280 Further integration of this 3D-MSI probes with ultrahigh resolution instruments and tandem MS  
36  
37  
38 281 strategies will provide independent verification of the molecular composition at the single cell  
39  
40 282 level and increase the analytical power of 3D-SIMS. The high homogeneity across the follicles  
41  
42 283 (Figure 1) between the two feeding conditions allows to more confidently extrapolate the 3D-TOF-  
43  
44  
45 284 SIMS results ( $n=2$  per feeding condition).

46  
47  
48 285 **Conflicts of interest**

49  
50 286 The authors report that there are no conflicts of interest.  
51  
52  
53  
54  
55  
56  
57  
58  
59  
60

1  
2  
3 **287 Acknowledgements**  
4

5 288 This work was supported by the NIH grant No. R21AI135469-01A1 to FFL. AC was fully  
6  
7 289 supported by NRC Fellowship NRC-HQ-84-14-G-0040 as well as by NSF grant HRD-1547798  
8  
9  
10 290 through a Fellowship offered by FIUs Centers of Research Excellence in Science and Technology  
11  
12 291 (CREST) program over the course of this study. This is contribution number ### from the  
13  
14 292 Southeast Environmental Research Center in the Institute of Water and Environment at Florida  
15  
16 293 International University. The authors thank Dan Graham, Ph.D., for developing the NESAC/BIO  
17  
18  
19 294 Toolbox used in this study and NIH grant EB-002027 for supporting the toolbox development.  
20  
21  
22  
23  
24  
25  
26  
27  
28  
29  
30  
31  
32  
33  
34  
35  
36  
37  
38  
39  
40  
41  
42  
43  
44  
45  
46  
47  
48  
49  
50  
51  
52  
53  
54  
55  
56  
57  
58  
59  
60

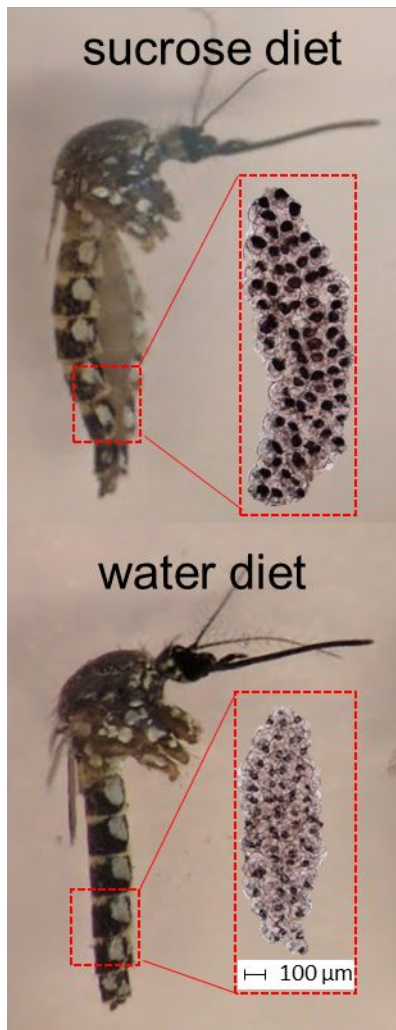
297 **Table 1.** Tentative assignments of signals observed in 3D-TOF-SIMS analysis of *Ae. aegypti* ovarian follicles.  
 298 LC-MS/MS assignments were manually curated and a 10 ppm tolerance was used for the parent ion  
 299 database search.

TOF SIMS $m/z$	Tentative Assignment	Proposed Chemical Formula	Theoretical $m/z$	LC-MS/MS
730.5	PC 32:2 (16:1/16:1) [M+H] <sup>+</sup>	C <sub>40</sub> H <sub>77</sub> NO <sub>8</sub> P	730.5381	HG-H <sub>2</sub> O 166.066, HG 184.0801, M-16:1-H <sub>2</sub> O 476.3152, M-NL 547.4637, M-C <sub>5</sub> H <sub>13</sub> NO <sub>3</sub> P-H <sub>2</sub> O 547.4637
732.4	PC 32:1 (16:0/16:1) [M+H] <sup>+</sup>	C <sub>40</sub> H <sub>79</sub> NO <sub>8</sub> P	732.5538	C <sub>5</sub> H <sub>13</sub> N 86.1116, M-C <sub>35</sub> H <sub>65</sub> O <sub>7</sub> P-H <sub>2</sub> O 86.1116, HG-H <sub>2</sub> O 166.0694, HG 184.0799, M-16:0-H <sub>2</sub> O 476.3183, M-16:1-H <sub>2</sub> O 478.3238
734.4	PC 32:0 (16:0/16:0) [M+H] <sup>+</sup>	C <sub>40</sub> H <sub>81</sub> NO <sub>8</sub> P	734.5694	M-16:0-H <sub>2</sub> O 478.2291, M-C <sub>2</sub> H <sub>6</sub> N 691.4202, M 734.463
756.5	PC 34:3 (16:1/18:2) [M+H] <sup>+</sup>	C <sub>42</sub> H <sub>79</sub> NO <sub>8</sub> P	756.5538	HG-H <sub>2</sub> O 166.0788, HG 184.0801, 15:1 C=O <sup>+</sup> 237.2243, M-18:2-H <sub>2</sub> O 476.3126, M-16:1-H <sub>2</sub> O 502.3297, M-16:1 520.3345
758.4	PC 34:2 [M+H] <sup>+</sup>	C <sub>42</sub> H <sub>81</sub> NO <sub>8</sub> P	758.5694	HG-H <sub>2</sub> O 166.0686, HG 184.0787
760.4	PC 34:1 (16:0/18:1) M+H] <sup>+</sup>	C <sub>42</sub> H <sub>83</sub> NO <sub>8</sub> P	760.5851	HG-H <sub>2</sub> O 166.0704, HG 184.0799, M-18:1-H <sub>2</sub> O 478.3262, M-18:1 496.3315, M-16:0-H <sub>2</sub> O 504.3437
786.4	PC 36:2 (18:1/18:1) [M+H] <sup>+</sup>	C <sub>44</sub> H <sub>85</sub> NO <sub>8</sub> P	786.6007	HG-H <sub>2</sub> O 166.0671, HG 184.0796, 17:1 C=O <sup>+</sup> 265.2517, M-18:1-H <sub>2</sub> O 504.3393, M-18:1 522.359, M-NL 603.544, M-C <sub>5</sub> H <sub>13</sub> NO <sub>3</sub> P-H <sub>2</sub> O 603.544
823.6	TG 48:3 (16:1/16:1/16:1) [M+Na] <sup>+</sup>	C <sub>51</sub> H <sub>92</sub> O <sub>6</sub> Na	823.6786	M-16:1 569.4508
	TG 48:3 (14:1/16:1/18:1) [M+Na] <sup>+</sup>	C <sub>51</sub> H <sub>92</sub> O <sub>6</sub> Na	823.6786	15:1 C=O <sup>+</sup> 237.2207, M-18:1 519.4371, M-18:1 541.4167, M-16:1 547.4674, M-14:1 575.4999, M 823.6528
825.6	TG 48:2 (16:0/16:1/16:1) [M+Na] <sup>+</sup>	C <sub>51</sub> H <sub>94</sub> O <sub>6</sub> Na	825.6943	15:1 C=O <sup>+</sup> 237.2268, 15:0 C=O <sup>+</sup> 239.2386, M-16:0 547.4672, M-16:1 549.482, M-16:0 569.4498, M-16:1 571.4654, M 825.6911
827.6	TG 48:1 (16:0/16:0/16:1) [M+Na] <sup>+</sup>	C <sub>51</sub> H <sub>96</sub> O <sub>6</sub> Na	827.7099	15:1 C=O <sup>+</sup> 237.225, 15:0 C=O <sup>+</sup> 239.242, M-16:0 549.4849, M-16:1 551.4965, M-16:0 571.4674, M-16:1 573.4857
849.6	TG 50:4 [M+Na] <sup>+</sup>	C <sub>53</sub> H <sub>94</sub> O <sub>6</sub> Na	849.6943	
851.6	TG 50:3 (16:1/16:1/18:1) [M+Na] <sup>+</sup>	C <sub>53</sub> H <sub>96</sub> O <sub>6</sub> Na	851.7099	15:1 C=O <sup>+</sup> 237.2233, M-18:1 547.4704, M-16:1 575.5006, M-16:1 597.4813



853.6	TG 50:2 [M+Na] <sup>+</sup>	C <sub>53</sub> H <sub>98</sub> O <sub>6</sub> Na	853.7256	
855.6	TG 50:1 (16:0/16:1/18:0) [M+Na] <sup>+</sup>	C <sub>53</sub> H <sub>100</sub> O <sub>6</sub> Na	855.7412	M-18:0 549.4957, M-16:1 579.5271
	TG 50:1 (16:0/16:0/18:1) [M+Na] <sup>+</sup>	C <sub>53</sub> H <sub>100</sub> O <sub>6</sub> Na	855.7412	15:0 C=O <sup>+</sup> 239.2402, 17:1 C=O <sup>+</sup> 265.2562, M-18:1 551.4988, M-18:1 573.4829, M-16:0 577.5165, M-16:0 599.4967, M 855.7492
877.6	TG 52:4 [M+Na] <sup>+</sup>	C <sub>55</sub> H <sub>98</sub> O <sub>6</sub> Na	877.7256	
879.6	TG 52:3 [M+Na] <sup>+</sup>	C <sub>55</sub> H <sub>100</sub> O <sub>6</sub> Na	879.7436	15:1 C=O <sup>+</sup> 237.2205, 17:1 C=O <sup>+</sup> 265.2538, M-20:4 575.5001, M-18:1 597.4808, M-16:1 625.5152, M 879.7376
881.7	TG 52:2 (16:1/18:0/18:1) [M+Na] <sup>+</sup>	C <sub>55</sub> H <sub>102</sub> O <sub>6</sub> Na	881.7569	15:1 C=O <sup>+</sup> 237.2273, 17:1 C=O <sup>+</sup> 265.2519, 17:0 C=O <sup>+</sup> 267.2516, M-18:0 575.4972, M-18:1 577.5128, M-18:0 597.4911, M-18:1 599.5001, M-16:1 605.5454, M-16:1 627.5321, M 881.7615
883.7	TG 52:1 (16:0/16:1/20:0) [M+Na] <sup>+</sup>	C <sub>55</sub> H <sub>104</sub> O <sub>6</sub> Na	883.7725	15:1 C=O <sup>+</sup> 237.2269, 15:0 C=O <sup>+</sup> 239.2438, M-20:0 549.4856, M-20:0 571.4671, M-16:0 605.5491, M-16:1 607.5609, M-16:0 627.5306, M-16:1 629.5331, M 883.7721
905.7	TG 54:4 [M+Na] <sup>+</sup>	C <sub>57</sub> H <sub>102</sub> O <sub>6</sub> Na	905.7569	
907.7	TG 54:3 [M+Na] <sup>+</sup>	C <sub>57</sub> H <sub>104</sub> O <sub>6</sub> Na	907.7725	
909.7	TG 54:2 [M+Na] <sup>+</sup>	C <sub>57</sub> H <sub>106</sub> O <sub>6</sub> Na	909.7882	

300

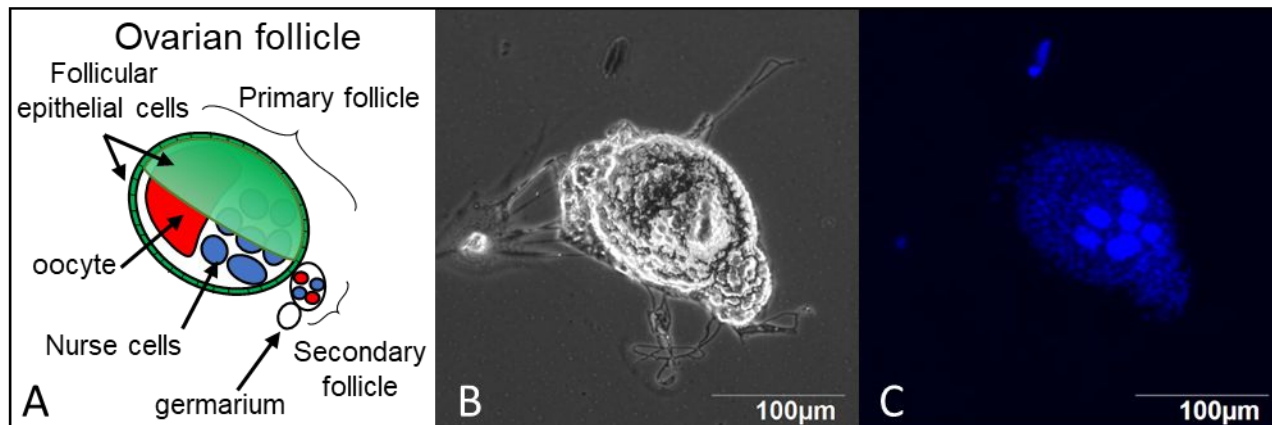


301

302 Figure 1. Optical images of 5-day old adult *Ae. aegypti*. The ovaries of the sucrose-fed female are  
303 larger than the water-fed counterpart.

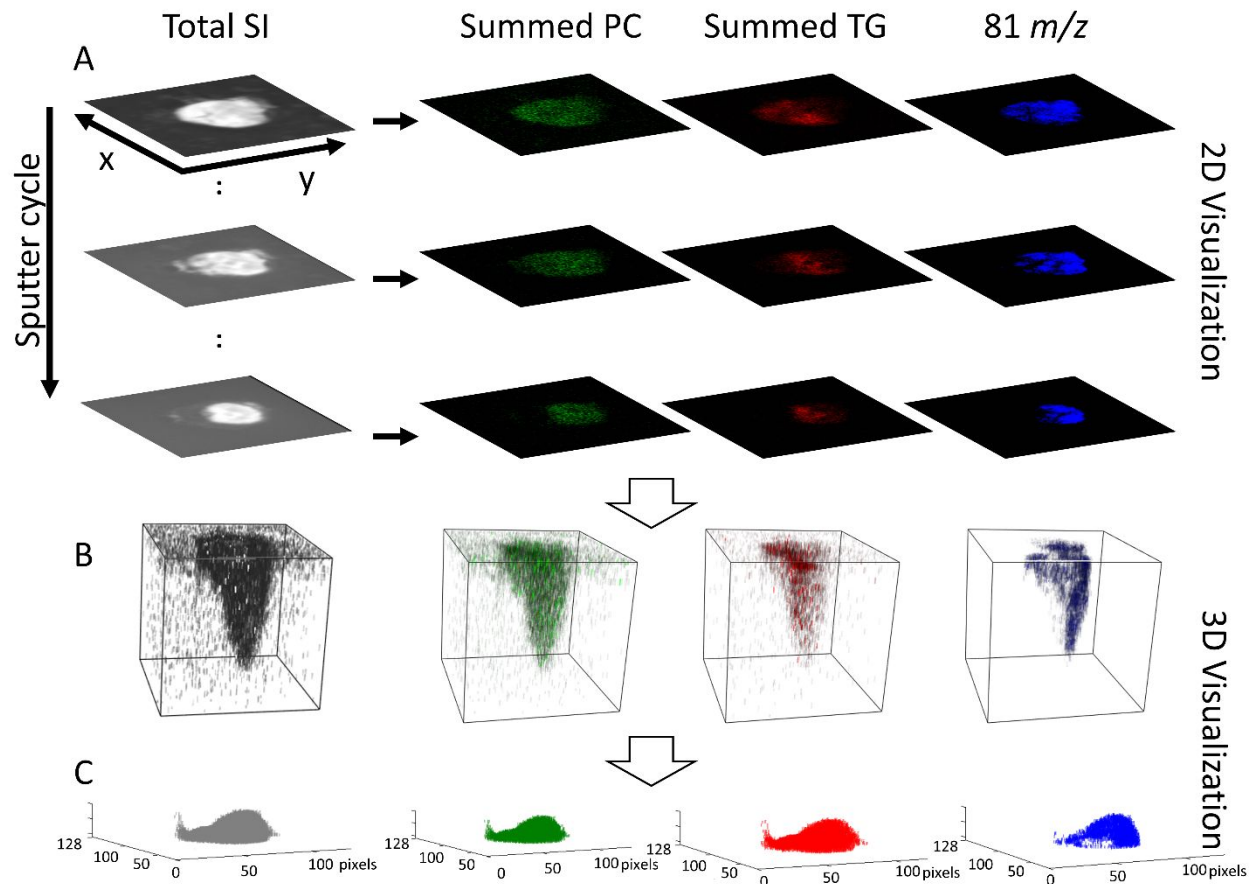
304

305



306

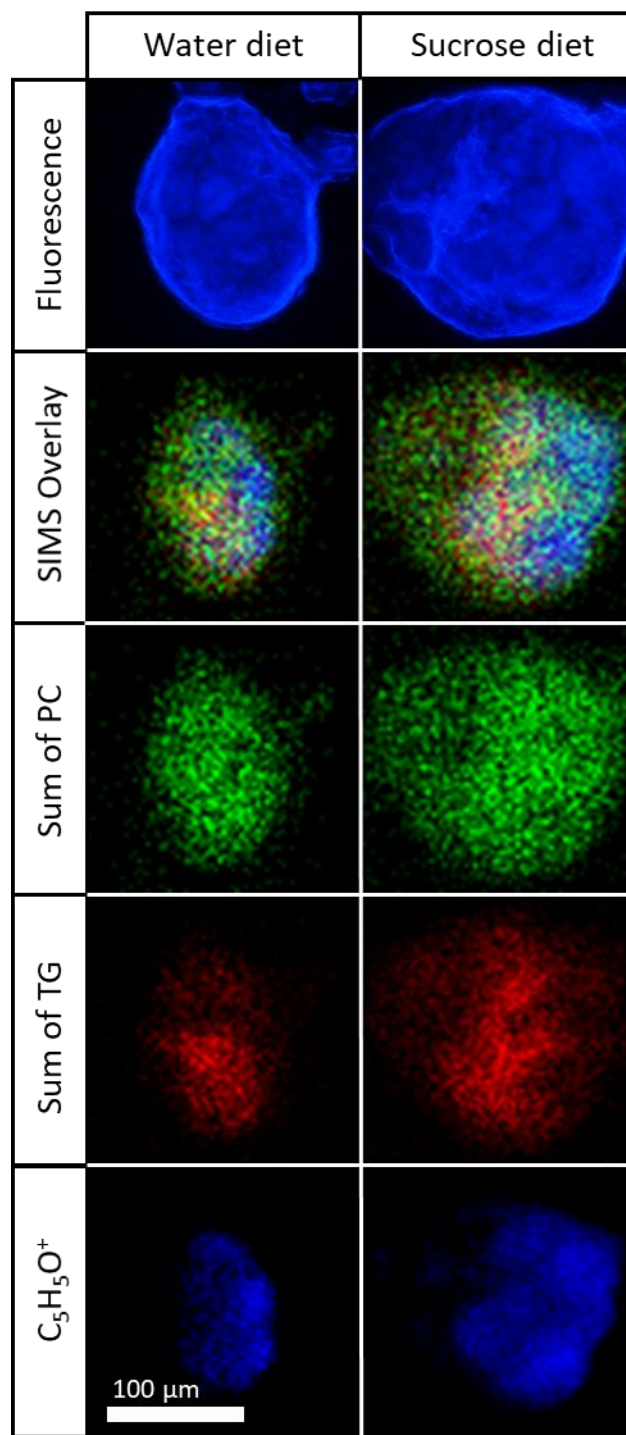
307 Figure 2. (A) Schematic, (B) optical, and (C) fluorescence images of a previtellogenic ovarian  
308 follicle of *Ae. aegypti*. Each follicle consists of one oocyte plus 7 nurse cells that are surrounded  
309 by follicular epithelial cells. A secondary follicle and the germarium are also visualized distal to  
310 the oocyte.



311

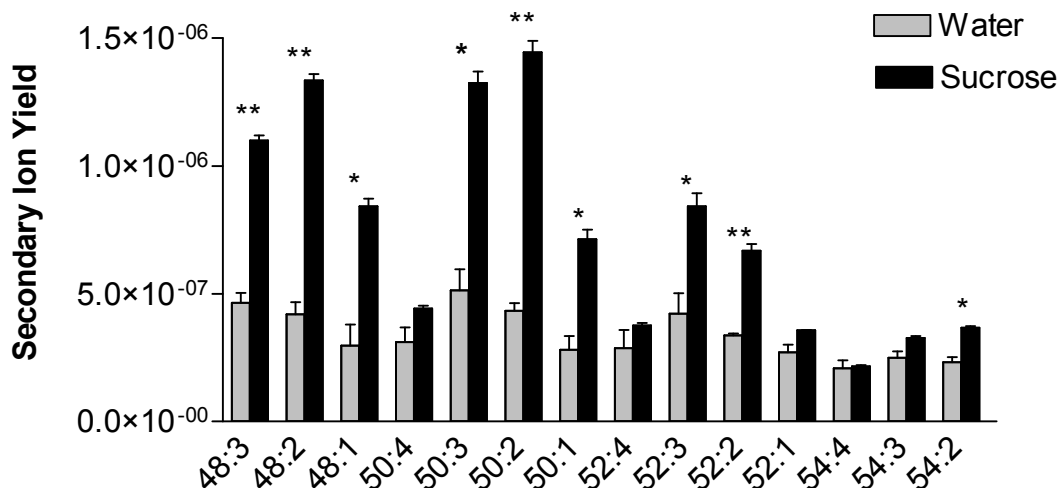
312 Figure 3. Visualization of the 3D-MSI analysis of freeze-dried ovarian follicle from a sucrose-diet  
 313 insect using dual beam TOF-SIMS. (A) 2D slices showing phosphatidylcholine (PC),  
 314 triacylglyceride (TG) and ribose (81  $m/z$ ), (B) 3D-MSI composite, and (C) software corrected 3D  
 315 reconstruction of non-flat surfaces. The 2D representations correspond to a field of view of  
 316 200x200  $\mu\text{m}$ . In (C), the x and y axis are shown in pixels (1 pixel = 1.56  $\mu\text{m}$ ).

317



319 Figure 4. Fluorescence and overlay of all 2D images from the 3D-MSI analysis (top view) of  
320 follicles from water- and sucrose-diet mosquitoes. DAPI staining allows fluorescence imaging of  
321 nurse cells. Secondary ion signal from selected  $m/z$  were used to visualize the distribution of

322 phosphatidylcholine (PC), triacylglyceride (TG), and ribose within individual follicles. A typical  
 323 SIMS spectrum is shown in Figure S3.



324  
 325  
 326 Figure 5. Comparison of the sum triacylglyceride (TG) signal from the 3D-MSI analysis. The  
 327 analysis was comprised of n=2 individual follicles from a single water-fed, and a single sucrose-  
 328 fed female. Bars represent the mean and the standard error of the mean (SEM) of duplicate  
 329 measurements. Asterisks denote significant difference (unpaired t-test: \*\* p<=0.01, \* p<=0.05).

330  
 331  
 332  
 333  
 334  
 335  
 336

337

338

339

## 340 References

341 [1] T. Hu, J.-L. Zhang, Mass-spectrometry-based lipidomics, *Journal of Separation Science*, 41 (2017) 351-  
342 372.

343 [2] Y.H. Rustam, G.E. Reid, Analytical Challenges and Recent Advances in Mass Spectrometry Based  
344 Lipidomics, *Analytical Chemistry*, 90 (2018) 374-397.

345 [3] R. Bandu, H.J. Mok, K.P. Kim, Phospholipids as cancer biomarkers: Mass spectrometry-based analysis,  
346 *Mass Spectrometry Reviews*, 37 (2016) 107-138.

347 [4] C.Z. Ulmer, R.A. Yost, J. Chen, C.E. Mathews, T.J. Garrett, Liquid chromatography-mass spectrometry  
348 metabolic and lipidomic sample preparation workflow for suspension-cultured mammalian cells using  
349 Jurkat T lymphocyte cells, *J. Proteomics Bioinf.*, 8 (2015) 360/361-360/367.

350 [5] D. Veličković, R.K. Chu, A.A. Carrell, M. Thomas, L. Paša-Tolić, D.J. Weston, C.R. Anderton, Multimodal  
351 MSI in Conjunction with Broad Coverage Spatially Resolved MS2 Increases Confidence in Both Molecular  
352 Identification and Localization, *Analytical Chemistry*, 90 (2018) 702-707.

353 [6] G.J. Van Berkel, V. Kertesz, K.A. Koeplinger, M. Vavrek, A.-N.T. Kong, Liquid microjunction surface  
354 sampling probe electrospray mass spectrometry for detection of drugs and metabolites in thin tissue  
355 sections, *Journal of Mass Spectrometry*, 43 (2007) 500-508.

356 [7] Z. Takáts, J.M. Wiseman, B. Gologan, R.G. Cooks, Mass Spectrometry Sampling Under Ambient  
357 Conditions with Desorption Electrospray Ionization, *Science*, 306 (2004) 471.

358 [8] R.G. Cooks, Z. Ouyang, Z. Takats, J.M. Wiseman, Ambient Mass Spectrometry, *Science*, 311 (2006)  
359 1566.

360 [9] G.J. Van Berkel, A.D. Sanchez, J.M.E. Quirke, Thin-Layer Chromatography and Electrospray Mass  
361 Spectrometry Coupled Using a Surface Sampling Probe, *Analytical Chemistry*, 74 (2002) 6216-6223.

362 [10] D.I. Campbell, C.R. Ferreira, L.S. Eberlin, R.G. Cooks, Improved spatial resolution in the imaging of  
363 biological tissue using desorption electrospray ionization, *Analytical and Bioanalytical Chemistry*, 404  
364 (2012) 389-398.

365 [11] L. Lamont, G.B. Eijkel, E.A. Jones, B. Flinders, S.R. Ellis, T. Porta, R.M.A. Heeren, R.J. Vreeken,  
366 Targeted Drug and Metabolite Imaging: Desorption Electrospray Ionization combined with Triple  
367 Quadrupole Mass Spectrometry, *Analytical Chemistry*, DOI 10.1021/acs.analchem.8b03857(2018).

368 [12] R. Yin, J. Kyle, K. Burnum-Johnson, K.J. Bloodsworth, L. Sussel, C. Ansong, J. Laskin, High Spatial  
369 Resolution Imaging of Mouse Pancreatic Islets Using Nanospray Desorption Electrospray Ionization Mass  
370 Spectrometry, *Analytical Chemistry*, 90 (2018) 6548-6555.

371 [13] A. Zavalin, J. Yang, K. Hayden, M. Vestal, R.M. Caprioli, Tissue protein imaging at 1  $\mu\text{m}$  laser spot  
372 diameter for high spatial resolution and high imaging speed using transmission geometry MALDI TOF  
373 MS, *Analytical and Bioanalytical Chemistry*, 407 (2015) 2337-2342.

374 [14] M. Karas, F. Hillenkamp, Laser desorption ionization of proteins with molecular masses exceeding  
375 10,000 daltons, *Analytical Chemistry*, 60 (1988) 2299-2301.

376 [15] R.M. Caprioli, T.B. Farmer, J. Gile, Molecular Imaging of Biological Samples: Localization of Peptides  
377 and Proteins Using MALDI-TOF MS, *Anal. Chem.*, 69 (1997) 4751-4760.

378 [16] T.C. Baker, J. Han, C.H. Borchers, Recent advancements in matrix-assisted laser  
379 desorption/ionization mass spectrometry imaging, *Curr. Opin. Biotechnol.*, 43 (2017) 62-69.

380 [17] E. Gemperline, S. Rawson, L. Li, Optimization and Comparison of Multiple MALDI Matrix Application  
381 Methods for Small Molecule Mass Spectrometric Imaging, *Analytical Chemistry*, 86 (2014) 10030-10035.

- 1  
2  
3 382 [18] Q.P. Vanbellingen, A. Castellanos, M. Rodriguez-Silva, I. Paudel, J.W. Chambers, F.A. Fernandez-  
4 383 Lima, Analysis of Chemotherapeutic Drug Delivery at the Single Cell Level Using 3D-MSI-TOF-SIMS,  
5 384 Journal of The American Society for Mass Spectrometry, 27 (2016) 2033-2040.
- 6 385 [19] A. Henss, S.-K. Otto, K. Schaepe, L. Pauksch, K.S. Lips, M. Rohnke, High resolution imaging and 3D  
7 386 analysis of Ag nanoparticles in cells with ToF-SIMS and delayed extraction, *Biointerphases*, 13 (2018)  
8 387 03B410.
- 9 388 [20] S. Sämfors, M. Ståhlman, M. Klevstig, J. Borén, J.S. Fletcher, Localised lipid accumulation detected in  
10 389 infarcted mouse heart tissue using ToF-SIMS, *Int. J. Mass Spectrom.*, DOI  
11 390 [https://doi.org/10.1016/j.ijms.2017.09.012\(2017\)](https://doi.org/10.1016/j.ijms.2017.09.012(2017)).
- 12 391 [21] H. Tian, L.J. Sparvero, A.A. Amoscato, A. Bloom, H. Bayir, V.E. Kagan, N. Winograd, Gas Cluster Ion  
13 392 Beam Time-of-Flight Secondary Ion Mass Spectrometry High-Resolution Imaging of Cardiolipin  
14 393 Speciation in the Brain: Identification of Molecular Losses after Traumatic Injury, *Analytical Chemistry*,  
15 394 89 (2017) 4611-4619.
- 16 395 [22] S. Chandra, W.A. Ausserer, G.H. Morrison, Evaluation of matrix effects in ion microscopic analysis of  
17 396 freeze-fractured, freeze-dried cultured cells, *Journal of microscopy*, 148 (1987) 223-229.
- 18 397 [23] G. Slodzian, Étude d'une méthode d'analyse locale chimique et isotopique utilisant l'émission  
19 398 ionique secondaire, *Ann. Phys.*, 13 (1964) 591-648.
- 20 399 [24] A. Brunelle, D. Touboul, O. Laprevote, Biological tissue imaging with time-of-flight secondary ion  
21 400 mass spectrometry and cluster ion sources, *Journal of Mass Spectrometry*, 40 (2005) 985.
- 22 401 [25] D. Touboul, F. Halgand, A. Brunelle, R. Kersting, E. Tallarek, B. Hagenhoff, O. Laprevote, Tissue  
23 402 Molecular Ion Imaging by Gold Cluster Ion Bombardment, *Analytical Chemistry*, 76 (2004) 1550-1559.
- 24 403 [26] M.P. Seah, R. Havelund, I.S. Gilmore, Universal Equation for Argon Cluster Size-Dependence of  
25 404 Secondary Ion Spectra in SIMS of Organic Materials, *The Journal of Physical Chemistry C*, 118 (2014)  
26 405 12862-12872.
- 27 406 [27] E. Niehuis, R. Möllers, D. Rading, H.G. Cramer, R. Kersting, Analysis of organic multilayers and 3D  
28 407 structures using Ar cluster ions, *Surface and Interface Analysis*, 45 (2013) 158-162.
- 29 408 [28] M.P. Seah, Universal Equation for Argon Gas Cluster Sputtering Yields, *The Journal of Physical*  
30 409 *Chemistry C*, 117 (2013) 12622-12632.
- 31 410 [29] F.A. Fernandez-Lima, J. Post, J.D. DeBord, M.J. Eller, S.V. Verkhoturov, S. Della-Negra, A.S. Woods,  
32 411 E.A. Schweikert, Analysis of Native Biological Surfaces Using a 100 kV Massive Gold Cluster Source,  
33 412 *Analytical Chemistry*, 83 (2011) 8448-8453.
- 34 413 [30] K.J. Adams, J.D. DeBord, F. Fernandez-Lima, Lipid specific molecular ion emission as a function of  
35 414 the primary ion characteristics in TOF-SIMS, *Journal of Vacuum Science & Technology B*, 34 (2016)  
36 415 051804.
- 37 416 [31] M.G. Blain, S. Della-Negra, H. Joret, Y. Le Beyec, E.A. Schweikert, Secondary-ion yields from surfaces  
38 417 bombarded with keV molecular and cluster ions, *Physical Review Letters*, 63 (1989) 1625.
- 39 418 [32] R.D. Harris, N.J. Vanstipdonk, E.A. Schweikert, keV Cluster Impacts: Prospects for Cluster-SIMS, *Int.*  
40 419 *J. Mass Spectrom. Ion Proc.*, 174 (1998) 167-177.
- 41 420 [33] S. Della-Negra, J. Depauw, C. Guillermier, E.A. Schweikert, Massive clusters: Secondary emission  
42 421 from qkeV to qMeV. New emission processes? New SIMS probe?, *Surface and Interface Analysis*, 43  
43 422 (2011) 62-65.
- 44 423 [34] J.S. Fletcher, N.P. Lockyer, S. Vaidyanathan, J.C. Vickerman, TOF-SIMS 3D Biomolecular Imaging of  
45 424 *Xenopus laevis* Oocytes Using Buckminsterfullerene (C60) Primary Ions, *Analytical Chemistry*, 79 (2007)  
46 425 2199-2206.
- 47 426 [35] D. Weibel, S. Wong, N. Lockyer, P. Blenkinsopp, R. Hill, J.C. Vickerman, A C60 Primary Ion Beam  
48 427 System for Time of Flight Secondary Ion Mass Spectrometry: Its Development and Secondary Ion Yield  
49 428 Characteristics, *Analytical Chemistry*, 75 (2003) 1754-1764.



- 1  
2  
3 429 [36] M.J. van Stipdonk, R.D. Harris, E.A. Schweikert, A Comparison of Desorption Yields from C+60 to  
4 430 Atomic and Polyatomic Projectiles at keV Energies, *Rapid Communications in Mass Spectrometry*, 10  
5 431 (1996) 1987-1991.
- 6 432 [37] S. Ninomiya, K. Ichiki, H. Yamada, Y. Nakata, T. Seki, T. Aoki, J. Matsuo, Molecular depth profiling of  
7 433 multilayer structures of organic semiconductor materials by secondary ion mass spectrometry with large  
8 434 argon cluster ion beams, *Rapid Communications in Mass Spectrometry*, 23 (2009) 3264-3268.
- 9 435 [38] K. Moritani, M. Hashinokuchi, J. Nakagawa, T. Kashiwagi, N. Toyoda, K. Mochiji, Extremely low-  
10 436 energy projectiles for SIMS using size-selected gas cluster ions, *Appl. Surf. Sci.*, 255 (2008) 948-950.
- 11 437 [39] S. Sheraz née Rabbani, A. Barber, J.S. Fletcher, N.P. Lockyer, J.C. Vickerman, Enhancing secondary  
12 438 ion yields in time of flight-secondary ion mass spectrometry using water cluster primary beams,  
13 439 *Analytical chemistry*, 85 (2013) 5654-5658.
- 14 440 [40] H. Tian, D. Maciążek, Z. Postawa, B.J. Garrison, N. Winograd, CO<sub>2</sub> Cluster Ion Beam, an Alternative  
15 441 Projectile for Secondary Ion Mass Spectrometry, *Journal of the American Society for Mass Spectrometry*,  
16 442 27 (2016) 1476-1482.
- 17 443 [41] C. Bich, R. Havelund, R. Moellers, D. Touboul, F. Kollmer, E. Niehuis, I.S. Gilmore, A. Brunelle, Argon  
18 444 Cluster Ion Source Evaluation on Lipid Standards and Rat Brain Tissue Samples, *Anal. Chem.*  
19 445 (Washington, DC, U. S.), 85 (2013) 7745.
- 20 446 [42] S.M. Khalil, A. Roempp, J. Pretzel, K. Becker, B. Spengler, Phospholipid Topography of Whole-Body  
21 447 Sections of the *Anopheles stephensi* Mosquito, Characterized by High-Resolution Atmospheric-Pressure  
22 448 Scanning Microprobe Matrix-Assisted Laser Desorption/Ionization Mass Spectrometry Imaging, *Anal.*  
23 449 *Chem.* (Washington, DC, U. S.), 87 (2015) 11309-11316.
- 24 450 [43] T.N. Phan Nhu, S. Fletcher John, P. Sjövall, G. Ewing Andrew, ToF - SIMS imaging of lipids and lipid  
25 451 related compounds in *Drosophila* brain, *Surface and Interface Analysis*, 46 (2014) 123-126.
- 26 452 [44] D. Bhandari, M. Schott, A. Römpf, A. Vilcinskas, B. Spengler, Metabolite localization by atmospheric  
27 453 pressure high-resolution scanning microprobe matrix-assisted laser desorption/ionization mass  
28 454 spectrometry imaging in whole-body sections and individual organs of the rove beetle *Paederus riparius*,  
29 455 *Analytical & Bioanalytical Chemistry*, 407 (2015) 2189-2201.
- 30 456 [45] F. Kaftan, V. Vrkošlav, P. Kynast, P. Kulkarni, S. Böcker, J. Cvačka, M. Knaden, A. Svatoš, Mass  
31 457 spectrometry imaging of surface lipids on intact *Drosophila melanogaster* flies, *Journal of Mass*  
32 458 *Spectrometry*, 49 (2014) 223-232.
- 33 459 [46] G. Zhou, J.E. Pennington, M.A. Wells, Utilization of pre-existing energy stores of female *Aedes*  
34 460 *aegypti* mosquitoes during the first gonotrophic cycle, *Insect Biochem. Mol. Biol.*, 34 (2004) 919-925.
- 35 461 [47] H. Briegel, I. Knusel, S.E. Timmermann, *Aedes aegypti*: size, reserves, survival, and flight potential, *J*  
36 462 *Vector Ecol*, 26 (2001) 21-31.
- 37 463 [48] H.H. Hagedorn, The Control of Vitellogenesis in the Mosquito, *Aedes aegypti*, *American Zoologist*,  
38 464 14 (1974) 1207-1217.
- 39 465 [49] S. Bhatt, P.W. Gething, O.J. Brady, J.P. Messina, A.W. Farlow, C.L. Moyes, J.M. Drake, J.S.  
40 466 Brownstein, A.G. Hoen, O. Sankoh, M.F. Myers, D.B. George, T. Jaenisch, G.R.W. Wint, C.P. Simmons,  
41 467 T.W. Scott, J.J. Farrar, S.I. Hay, The global distribution and burden of dengue, *Nature*, 496 (2013) 504.
- 42 468 [50] S.C. Weaver, W.K. Reisen, Present and future arboviral threats, *Antiviral Research*, 85 (2010) 328-  
43 469 345.
- 44 470 [51] D. Musso, D.J. Gubler, Zika Virus, *Clinical Microbiology Reviews*, 29 (2016) 487.
- 45 471 [52] R.G.A. Feachem, A.A. Phillips, J. Hwang, C. Cotter, B. Wielgosz, B.M. Greenwood, O. Sabot, M.H.  
46 472 Rodriguez, R.R. Abeyasinghe, T.A. Ghebreyesus, R.W. Snow, Shrinking the malaria map: progress and  
47 473 prospects, *The Lancet*, 376 (2010) 1566-1578.
- 48 474 [53] A.N. Clements, *The biology of mosquitoes. Development, nutrition and reproduction*, CABI  
49 475 Publishing, New York, NY, 1992.

- 1  
2  
3 476 [54] M.J. Klowden, Endocrine aspects of mosquito reproduction, *Archives of Insect Biochemistry and*  
4 477 *Physiology*, 35 (1997) 491-512.
- 5 478 [55] M.E. Clifton, F.G. Noriega, Nutrient limitation results in juvenile hormone-mediated resorption of  
6 479 previtellogenic ovarian follicles in mosquitoes, *Journal of Insect Physiology*, 57 (2011) 1274-1281.
- 7 480 [56] M.E. Clifton, F.G. Noriega, The fate of follicles after a blood meal is dependent on previtellogenic  
8 481 nutrition and juvenile hormone in *Aedes aegypti*, *Journal of Insect Physiology*, 58 (2012) 1007-1019.
- 9 482 [57] R. Ziegler, M.M. Ibrahim, Formation of lipid reserves in fat body and eggs of the yellow fever  
10 483 mosquito, *Aedes aegypti*, *Journal of Insect Physiology*, 47 (2001) 623-627.
- 11 484 [58] E. Van Handel, The obese mosquito, *The Journal of Physiology*, 181 (1965) 478-486.
- 12 485 [59] S. Chandra, G.H. Morrison, C.C. Wolcott, Imaging intracellular elemental distribution and ion fluxes  
13 486 in cultured cells using ion microscopy: a freeze-fracture methodology, *Journal of microscopy*, 144 (1986)  
14 487 15-37.
- 15 488 [60] E.S.F. Berman, S.L. Fortson, K.D. Checchi, L. Wu, J.S. Felton, K.J.J. Wu, K.S. Kulp, Preparation of single  
16 489 cells for imaging/profiling mass spectrometry, *Journal of the American Society for Mass Spectrometry*,  
17 490 19 (2008) 1230-1236.
- 18 491 [61] J. Malm, D. Giannaras, M.O. Riehle, N. Gadegaard, P. Sjövall, Fixation and Drying Protocols for the  
19 492 Preparation of Cell Samples for Time-of-Flight Secondary Ion Mass Spectrometry Analysis, *Analytical*  
20 493 *Chemistry*, 81 (2009) 7197-7205.
- 21 494 [62] J.S. Fletcher, S. Rabbani, A. Henderson, N.P. Lockyer, J.C. Vickerman, Three-dimensional mass  
22 495 spectral imaging of HeLa-M cells – sample preparation, data interpretation and visualisation, *Rapid*  
23 496 *Communications in Mass Spectrometry*, 25 (2011) 925-932.
- 24 497 [63] G.C. Atella, K.C. Gondim, E.A. Machado, M.N. Medeiros, M.A.C. Silva-Neto, H. Masuda, Oogenesis  
25 498 and egg development in triatomines: a biochemical approach, *An. Acad. Bras. Cienc.*, 77 (2005) 405-430.
- 26 499 [64] E. Van Handel, Fuel metabolism of the mosquito (*Culex quinquefasciatus*) embryo, *Journal of Insect*  
27 500 *Physiology*, 39 (1993) 831-833.
- 28 501 [65] H. Briegel, M. Hefti, E. DiMarco, Lipid metabolism during sequential gonotrophic cycles in large and  
29 502 small female *Aedes aegypti*, *Journal of Insect Physiology*, 48 (2002) 547-554.
- 30 503 [66] J.D. DeBord, D.F. Smith, C.R. Anderton, R.M. Heeren, L. Pasa-Tolic, R.H. Gomer, F.A. Fernandez-  
31 504 Lima, Secondary Ion Mass Spectrometry Imaging of *Dictyostelium discoideum* Aggregation Streams, *Plos*  
32 505 *One*, 9 (2014) e99319.
- 33 506 [67] S. Chandra, 3D subcellular SIMS imaging in cryogenically prepared single cells, *Appl. Surf. Sci.*, 231-  
34 507 232 (2004) 467-469.
- 35 508 [68] M.A. Robinson, D.J. Graham, D.G. Castner, ToF-SIMS Depth Profiling of Cells: z-Correction, 3D  
36 509 Imaging, and Sputter Rate of Individual NIH/3T3 Fibroblasts, *Analytical Chemistry*, 84 (2012) 4880-4885.
- 37 510 [69] C.F. Newman, R. Havelund, M.K. Passarelli, P.S. Marshall, I. Francis, A. West, M.R. Alexander, I.S.  
38 511 Gilmore, C.T. Dollery, Intracellular Drug Uptake—A Comparison of Single Cell Measurements Using ToF-  
39 512 SIMS Imaging and Quantification from Cell Populations with LC/MS/MS, *Analytical Chemistry*, 89 (2017)  
40 513 11944-11953.
- 41 514 [70] A.N. Rao, N. Vandencastele, L.J. Gamble, D.W. Grainger, High resolution epifluorescence and TOF-  
42 515 SIMS chemical imaging comparisons of single DNA microarray spots, *Analytical chemistry*, 84 (2012)  
43 516 10628-10636.
- 44 517 [71] C.J. May, H.E. Canavan, D.G. Castner, Quantitative X-ray Photoelectron Spectroscopy and Time-of-  
45 518 Flight Secondary Ion Mass Spectrometry Characterization of the Components in DNA, *Analytical*  
46 519 *Chemistry*, 76 (2004) 1114-1122.
- 47 520 [72] M.H. Perez, F.G. Noriega, *Aedes aegypti* pharate 1st instar quiescence affects larval fitness and  
48 521 metal tolerance, *Journal of insect physiology*, 58 (2012) 824-829.
- 49 522 [73] C.L. Boggs, C.L. Ross, The Effect of Adult Food Limitation on Life History Traits in *Speyeria Mormonia*  
50 523 (*Lepidoptera: Nymphalidae*), *Ecology*, 74 (1993) 433-441.

1  
2  
3  
4  
5  
6  
7  
8  
9  
10  
11  
12  
13  
14  
15  
16  
17  
18  
19  
20  
21  
22  
23  
24  
25  
26  
27  
28  
29  
30  
31  
32  
33  
34  
35  
36  
37  
38  
39  
40  
41  
42  
43  
44  
45  
46  
47  
48  
49  
50  
51  
52  
53  
54  
55  
56  
57  
58  
59  
60

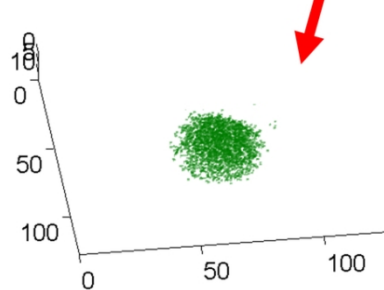
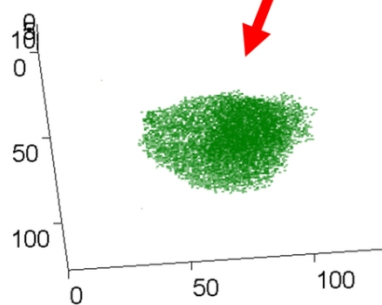
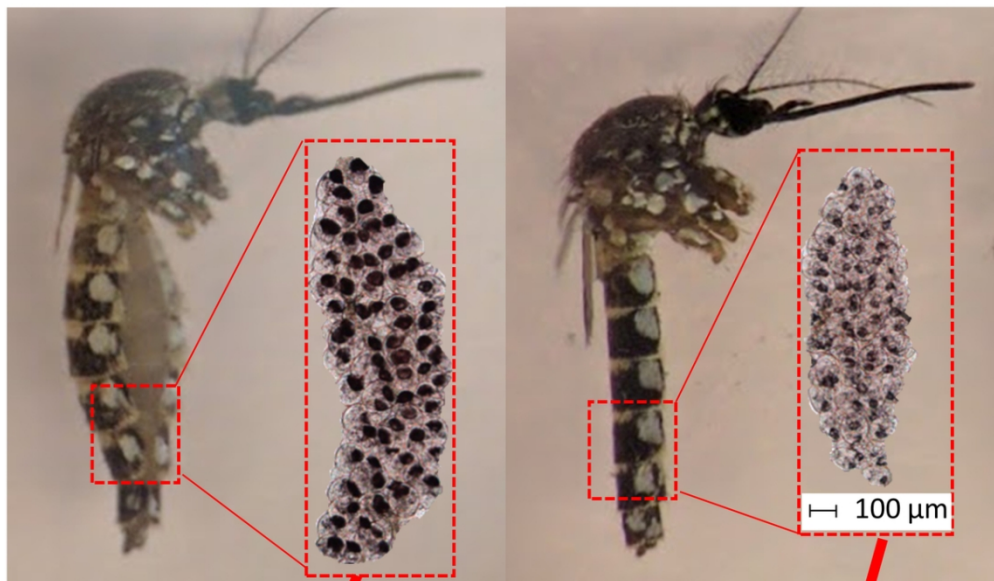
524

525

1  
2  
3  
4  
5  
6  
7  
8  
9  
10  
11  
12  
13  
14  
15  
16  
17  
18  
19  
20  
21  
22  
23  
24  
25  
26  
27  
28  
29  
30  
31  
32  
33  
34  
35  
36  
37  
38  
39  
40  
41  
42  
43  
44  
45  
46  
47  
48  
49  
50  
51  
52  
53  
54  
55  
56  
57  
58  
59  
60

sucrose diet

water diet



103x107mm (300 x 300 DPI)

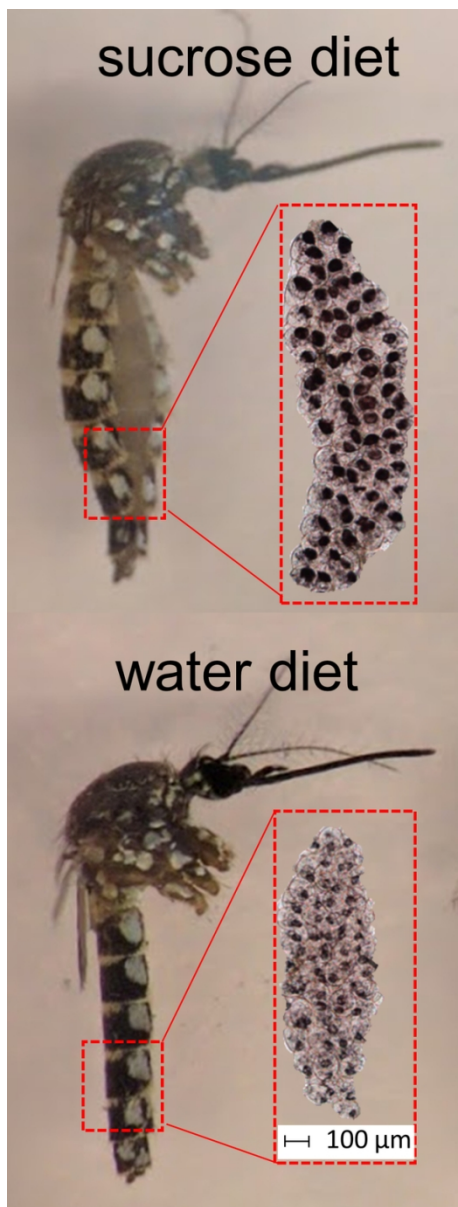


Figure 1

51x135mm (300 x 300 DPI)

1  
2  
3  
4  
5  
6  
7  
8  
9  
10  
11  
12  
13  
14  
15  
16  
17  
18  
19  
20  
21  
22  
23  
24  
25  
26  
27  
28  
29  
30  
31  
32  
33  
34  
35  
36  
37  
38  
39  
40  
41  
42  
43  
44  
45  
46  
47  
48  
49  
50  
51  
52  
53  
54  
55  
56  
57  
58  
59  
60

1  
2  
3  
4  
5  
6  
7  
8  
9  
10  
11  
12  
13  
14  
15  
16  
17  
18  
19  
20  
21  
22  
23  
24  
25  
26  
27  
28  
29  
30  
31  
32  
33  
34  
35  
36  
37  
38  
39  
40  
41  
42  
43  
44  
45  
46  
47  
48  
49  
50  
51  
52  
53  
54  
55  
56  
57  
58  
59  
60

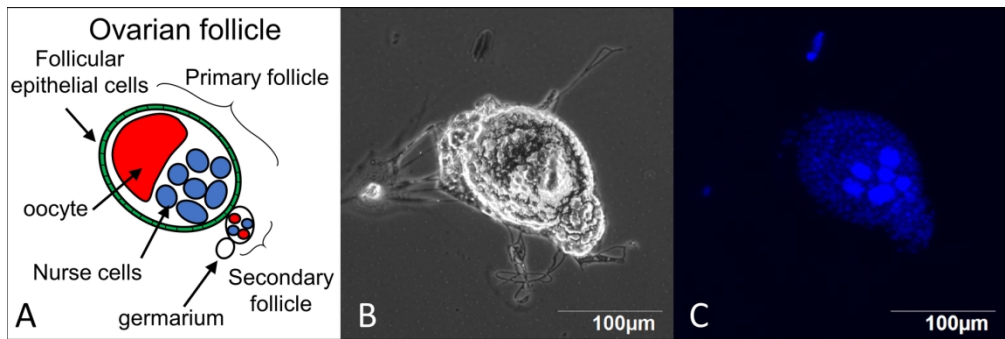


Figure 2

168x55mm (300 x 300 DPI)

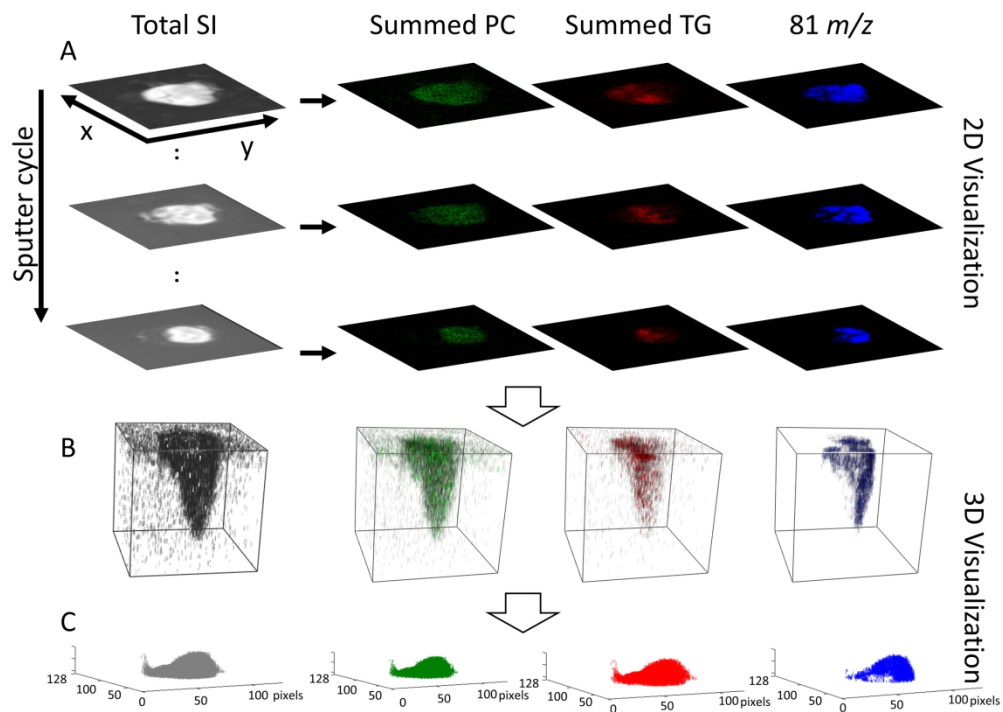


Figure 3

212x154mm (300 x 300 DPI)

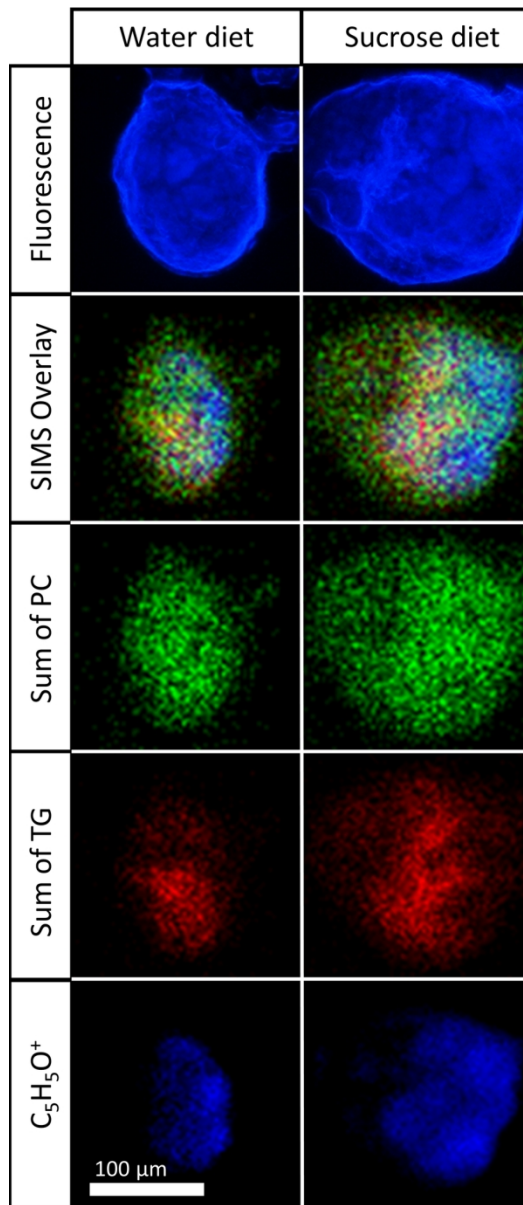


Figure 4

82x188mm (300 x 300 DPI)



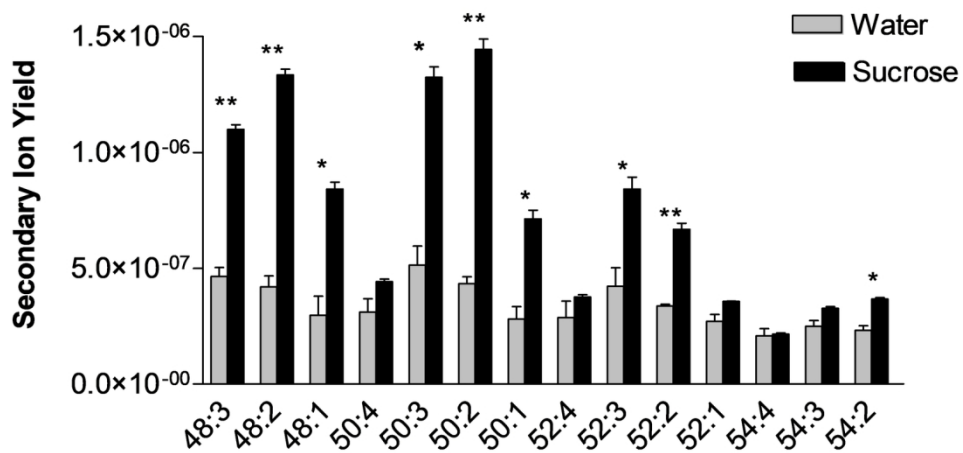


Fig 5

146x76mm (300 x 300 DPI)